2), which blocks both α_v integrins (*16*), showed the greatest antiangiogenic and antitumoral activity when compared with either anti-$\alpha_v\beta_3$ alone or anti-$\alpha_v\beta_5$ alone (*16*).

Most ocular diseases that cause catastrophic loss of vision have as a common pathologic feature the growth of new blood vessels. Although ischemia-associated retinal neovascular diseases such as proliferative diabetic retinopathy are associated with increased VEGF (*12*), nonischemic subretinal neovascular diseases such as age-related macular degeneration have no such clear association. Our observation that VEGF-stimulated angiogenesis proceeds by an integrin-mediated angiogenic pathway distinct from that stimulated by FGF supports the concept that different pathogenetic mechanisms may operate in retinal and subretinal diseases (*17*).

Angiogenesis is a critical biologic process and, as such, may depend on redundant molecular events that not only initiate blood vessel cell proliferation but also regulate the invasion and, ultimately, the differentiation of newly forming vessels. Redundancy in this process is supported by an experiment of nature, Glanzmann's thrombasthenia, in which individuals lacking expression of the β_3 integrin gene nevertheless develop fully mature blood vessels. Thus, an alternative angiogenic mechanism must exist in the absence of $\alpha_v\beta_3$. The evidence presented here suggests that $\alpha_v\beta_5$ can provide such a mechanism of biologic redundancy. We conclude that there are at least two cytokine-dependent pathways leading to angiogenesis in vivo, and these are distinguished by their dependency on specific α_v integrins and on the intracellular serine-threonine kinase PKC.

REFERENCES AND NOTES

1. J. Folkman and Y. Shing, *J. Biol. Chem.* **267**, 10931 (1992); P. A. D'Amore and R. W. Thompson, *Annu. Rev. Physiol.* **49**, 453 (1987); J. Folkman, *Nature Med.* **1**, 27 (1995); D. Ingber and J. Folkman, *Cell Biol.* **109**, 317 (1989); D. Weinstat-Saslow and P. Steeg, *FASEB J.* **8**, 401 (1994).
2. J. E. Meredith, B. Fazeli, M. A. Schwartz, *Mol. Biol. Cell.* **4**, 953 (1993).
3. P. C. Brooks, R. A. F. Clark, D. A. Cheresh, *Science* **264**, 569 (1994).
4. P. C. Brooks *et al.*, *Cell* **79**, 1157 (1994).
5. C. J. Drake, D. A. Cheresh, C. D. Little, *J. Cell Sci.* **108**, 2655 (1995).
6. D. A. Cheresh, *Proc. Natl. Acad. Sci. U.S.A.* **84**, 6471 (1987).
7. D. I. Leavesley, M. A. Schwartz, M. Rosenfeld, D. A. Cheresh, *J. Cell Biol.* **121**, 163 (1993).
8. J. Enenstein and R. H. Kramer, *J. Invest. Dermatol.* **103**, 381 (1994).
9. D. A. Cheresh, S. A. Berliner, V. Vicente, V. Z. Ruggeri, *Cell* **58**, 945 (1989).
10. P. A. D'Amore, *Invest. Ophthalmol. Vis. Sci.* **35**, 3974 (1994).
11. J. W. Miller *et al.*, *Am. J. Pathol.* **145**, 574 (1994).
12. L. P. Aiello *et al.*, *N. Engl. J. Med.* **331**, 1480 (1994).
13. R. J. D'Amato, M. S. Loughnan, E. Flynn, J. Folkman, *Proc. Natl. Acad. Sci. U.S.A.* **91**, 4082 (1994); R. Shaffer and M. Friedlander, in *NATO ASI on Molecular, Cellular, and Clinical Aspects of Angiogenesis*, M. E. Maragoudakis, Ed. (Plenum, New York, in press). We modified the Hydron pellets so that endotoxin-free antibody was incorporated directly into the pellet. Eyes were examined and photographed daily through a Wild operating microscope. Photographs were recorded on Kodak Ektachrome 64T slide film, and images were converted for computer-assisted quantitation with Molecular Analyst 1.1 software (Bio-Rad) after acquisition through a Model GS670 imaging densitometer.
14. M. Pfaff *et al.*, *J. Biol. Chem.* **269**, 20233 (1994).
15. R. L. Klemke, M. Yebra, E. M. Bayna, D. A. Cheresh, *J. Cell Biol.* **127**, 859 (1994).
16. P. C. Brooks and D. A. Cheresh, unpublished data.
17. M. Friedlander, paper presented at the Retina Society Meeting, Santa Fe, NM, 8 September 1995.

18. Supported by grants to M.F. from the Lions Sightfirst Diabetic Retinopathy Research Program of the American Diabetes Association, the Scripps Clinic Department of Academic Affairs Clinical Research Program, and the Ralwhbnbg Fund, and by grants to D.A.C. from the National Cancer Institute and the Heart, Lung, and Blood Institute at the National Institutes of Health. D.A.C. is a recipient of an American Cancer Society Faculty Research Award. We thank S. Fallon, M. Sugita, and M. Toth for helpful comments and suggestions. We also thank S. Goodman and A. Jonczyk (E. Merck, KGaA, Darmstadt) for providing peptides and supporting evidence that cyclic peptide RGDfV (EP 0578 083 A2) blocks both $\alpha_v\beta_3$ and $\alpha_v\beta_5$. Sucralfate (Carafate) was a gift of Marion–Merrell Dow Pharmaceuticals (Cincinnati, OH).

2 June 1995; accepted 26 September 1995

Essential Ca^{2+}-Binding Motif for Ca^{2+}-Sensitive Inactivation of L-Type Ca^{2+} Channels

Marita de Leon, Yan Wang, Lisa Jones, Edward Perez-Reyes, Xiangyang Wei, Tuck Wah Soong, Terry P. Snutch, David T. Yue*

Intracellular calcium (Ca^{2+}) inhibits the opening of L-type (α_{1C}) Ca^{2+} channels, providing physiological control of Ca^{2+} entry into a wide variety of cells. A structural determinant of this Ca^{2+}-sensitive inactivation was revealed by chimeric Ca^{2+} channels derived from parental α_{1C} and α_{1E} channels, the latter of which is a neuronal channel lacking Ca^{2+} inactivation. A consensus Ca^{2+}-binding motif (an EF hand), located on the α_{1C} subunit, was required for Ca^{2+} inactivation. Donation of the α_{1C} EF-hand region to the α_{1E} channel conferred the Ca^{2+}-inactivating phenotype. These results strongly suggest that Ca^{2+} binding to the α_{1C} subunit initiates Ca^{2+} inactivation.

L-type Ca^{2+} channels manifest Ca^{2+}-sensitive inactivation (*1*), a biological feedback mechanism in which elevation of intracellular Ca^{2+} concentration ($[Ca^{2+}]$) speeds channel inactivation. As L-type Ca^{2+} channels are widely distributed, this inactivation process influences many cellular activities, including neuroendocrine secretion (*2*), cardiac excitation-contraction coupling (*3*), and neuronal gene regulation (*4*). Although the existence of Ca^{2+} inactivation was demonstrated over a decade ago (*1*), its underlying molecular mechanism remains unknown. Competing candidates for the chemical "switch" that initiates inactivation include Ca^{2+}-induced (de)phosphorylation of the channel (*5*), Ca^{2+} activation of calmodulin (*6*), and direct Ca^{2+} binding to the channel (*7*). Recent work (*8–10*) favors the latter, but evidence to date has been debated. Here, we present molecular evidence suggesting that an EF-hand Ca^{2+}-binding motif (*11*), located on the α_{1C} subunit of the cardiac L-type Ca^{2+} channel, provides the Ca^{2+} binding site that initiates Ca^{2+}-sensitive inactivation.

L-type Ca^{2+} channels, expressed transiently in HEK 293 cells from complementary DNAs encoding α_{1C} (*12*) and β_{2a} (*13*) subunits (*14*), possessed Ca^{2+}-sensitive inactivation (Fig. 1, A through C). With 10 mM Ba^{2+} as the charge carrier, whole-cell α_{1C} currents (Fig. 1A, top) showed little inactivation during 300-ms test depolarizations, as expected from the high selectivity of Ca^{2+} inactivation for Ca^{2+} over Ba^{2+} (*1*). Average data confirmed that Ba^{2+} currents decayed only slightly over the entire range of test depolarizations; peak currents were just larger than residual currents (Fig. 1A, bottom). By contrast, specimen current records decayed much more with 10 mM external Ca^{2+} as charge carrier (Fig. 1B, top), which suggests the onset of Ca^{2+} inactivation. Averages of peak and residual

M. de Leon, Y. Wang, L. Jones, D. T. Yue, Program in Molecular and Cellular Systems Physiology, Department of Biomedical Engineering, Johns Hopkins University School of Medicine, 720 Rutland Avenue, Baltimore, MD 21205, USA.
E. Perez-Reyes, Department of Physiology, Loyola University Chicago, 2160 South First Avenue, Maywood, IL 60153, USA.
X. Wei, Institute for Molecular Medicine and Genetics, Medical College of Georgia, 1120 15th Street, Augusta, GA 30912, USA.
T. W. Soong and T. P. Snutch, Biotechnology Laboratory, University of British Columbia, Vancouver, British Columbia V6T 1Z3, Canada.
*To whom correspondence should be addressed.

current confirmed the enhancement of inactivation by Ca^{2+} (Fig. 1B, bottom).

To quantitate inactivation, we plotted r_{300}, the fraction of peak current remaining at the end of a 300-ms depolarization, as a function of voltage (Fig. 1C). The r_{300} relation with Ca^{2+} defined a U-shaped plot, providing a hallmark of Ca^{2+} inactivation (*10*). The low point of the curve coincided with maximal Ca^{2+} entry (compare Fig. 1B), and r_{300} turned upward with further depolarization as the driving force for Ca^{2+} entry dropped. The small, monotonic decline of r_{300} with Ba^{2+} (Fig. 1C) reflected a separate, voltage-sensitive inactivation (*10*). Because voltage- and Ca^{2+}-sensitive inactivation are approximately independent processes (*10*), the difference between Ca^{2+} and Ba^{2+} r_{300} values provided a direct measure of Ca^{2+} inactivation, as exemplified by the parameter f (*15*) (Fig. 1C).

In contrast, a homologous Ca^{2+} channel, expressed from α_{1E} (*16*) and β_{2a} (*13*) subunits, lacked Ca^{2+} inactivation (Fig. 1, D through F), thereby establishing the feasibility of chimeric channel analysis (*17, 18*). The α_{1E} subunit is the pore-forming constituent of a medium-threshold Ca^{2+} channel in neurons (*16*). The α_{1E} Ba^{2+} currents (Fig. 1D) appeared to inactivate at the same rate as Ca^{2+} currents (Fig. 1E), despite larger current amplitudes with Ca^{2+}. The absence of Ca^{2+} inactivation was confirmed quantitatively by identical r_{300} relations with Ca^{2+} and Ba^{2+} (Fig. 1F). Because inactivation was unchanged by reduction of external [Ba^{2+}] or [Ca^{2+}] to 3 mM (*19*), the shallow U shape of the r_{300} relation did not indicate a current-sensitive inactivation with equal selectivity for Ca^{2+} and Ba^{2+}.

We tested whether differences in the COOH-termini of α_{1C} and α_{1E} account for their distinct inactivation properties, because this region contains an EF-hand motif with a possible role in Ca^{2+} activation (*20*). The entire COOH-terminus of α_{1E} was substituted into α_{1C} (*21*), and the resulting $\alpha_{1CE\text{-}1}$ chimera (Fig. 2A) completely lacked Ca^{2+} inactivation. Its Ca^{2+} inactivation parameter f was ≈0 (Fig. 2A), clearly lower than the α_{1C} value (0.44) and indistinguishable from the α_{1E} value (≈0). Thus, the α_{1C} COOH-terminus appeared to be essential for Ca^{2+} inactivation.

To refine localization of the essential region, we deleted two-thirds of the COOH-terminus of α_{1C} from amino acid 1733 to the stop codon. The resulting construct, α_{1Cdel}, manifested the same degree of Ca^{2+} inactivation as α_{1C}, with nearly identical f values (Fig. 2A). Substituting only the proximal fourth of the α_{1C} COOH-terminus (amino acids 1510 to 1690) with the corresponding α_{1E} locus produced a chimeric Ca^{2+} channel ($\alpha_{1CE\text{-}2}$; Fig. 2A) that completely lacked Ca^{2+} inactivation ($f \approx 0$). These two results suggest that the proximal fourth of the α_{1C} COOH-terminus contained a necessary region for Ca^{2+} inactivation.

When only the EF-hand region of α_{1C} (amino acids 1510 to 1560) was replaced by the homologous α_{1E} sequence, Ca^{2+} inactivation was also absent ($f \approx 0$ for $\alpha_{1CE\text{-}3}$; Fig. 2A). Comparison of whole-cell Ca^{2+} and Ba^{2+} records emphasized the complete ablation of Ca^{2+} inactivation in $\alpha_{1CE\text{-}3}$ (Fig. 2B). Both sets of records were nearly flat; the Ca^{2+} records have been scaled to illustrate the similarity of kinetics. The r_{300} plots confirmed that inactivation was consistently small and identical for Ca^{2+} and Ba^{2+} (Fig. 2B) over a wide range of potentials. The results with $\alpha_{1CE\text{-}3}$ showed that the EF-hand motif of α_{1C} is necessary for Ca^{2+} inactivation, as long as the functional knockout did not arise from higher order conformational derangement of the chimeric channel.

The chimeric channel was not likely to have serious conformational problems for several reasons. First, nonspecific distortion would change other whole-cell properties; but the average current-voltage relation of $\alpha_{1CE\text{-}3}$ (Fig. 2B) was very similar to that of α_{1C} (Fig. 1, A and B), suggesting that activation was unaffected. In fact, activation and steady-state voltage inactivation of all chimeras with an α_{1C} backbone were closely similar to those of α_{1C}.

Second, substitution of portions (including the EF hand) of the α_{1C} COOH-terminus into α_{1E} conferred the Ca^{2+}-inactivating phenotype. In particular, donation of the entire α_{1C} COOH-terminus to the α_{1E} backbone yielded a chimeric $\alpha_{1EC\text{-}1}$ channel with a Ca^{2+} inactivation parameter (f) of 0.28 (Fig. 2C). Simple deletion of up to two-thirds of the distal COOH-terminus of $\alpha_{1EC\text{-}1}$ preserved the same degree of Ca^{2+} sensitivity ($\alpha_{1EC\text{-}1\Delta4}$ and $\alpha_{1EC\text{-}1\Delta3}$) (Fig. 2C). Currents from $\alpha_{1EC\text{-}1}$ illustrated the extent to which inactivation has been conferred to these constructs (Fig. 2D). Of particular relevance is the selective enhancement of Ca^{2+} current inactivation with larger currents, a distinctive property of Ca^{2+} inactivation (compare Fig. 1C and Fig. 2D). Further COOH-terminal truncation of more than ≈50 amino acids produced nonfunctional channels ($\alpha_{1EC\text{-}1\Delta2}$) (Fig. 2C), as would be expected from previous studies (*12*).

To determine whether smaller portions of the α_{1C} COOH-terminus sufficed to impart Ca^{2+} inactivation to the α_{1E} backbone, we substituted narrow stretches of α_{1C} containing the EF hand into full-length α_{1E}, yielding $\alpha_{1EC\text{-}2}$ and $\alpha_{1EC\text{-}3}$ (Fig. 2C). Donation of smaller α_{1C} segments failed to confer Ca^{2+} inactivation ($f \approx 0$ for $\alpha_{1EC\text{-}2}$ and $\alpha_{1EC\text{-}3}$) (Fig. 2C) (*22*). To retain native

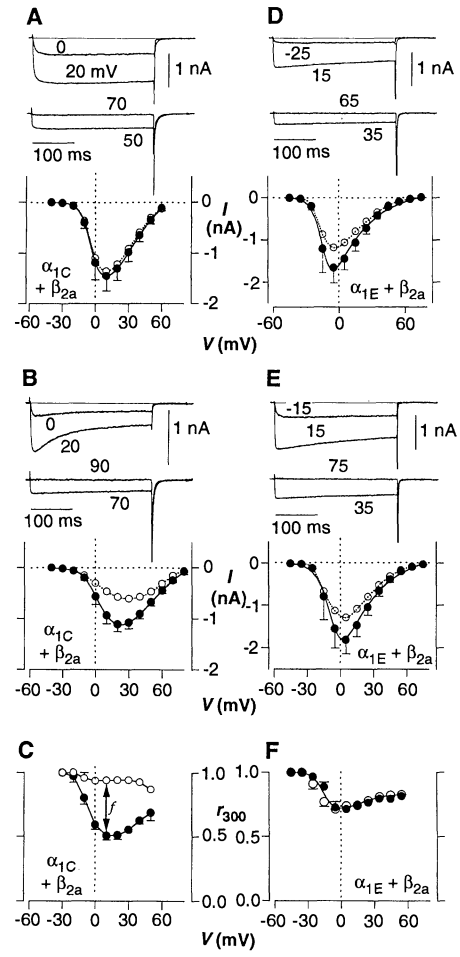

Fig. 1. Comparison of inactivation in α_{1C} and α_{1E}. (**A**) α_{1C} Ba^{2+} currents. Top, whole-cell records elicited by 300-ms depolarizations to the indicated potentials (0, 20, 70, and 50 mV). Holding potential was −60 mV; tail potential, −50 mV in a Cs-aspartate internal solution (*14*). Bottom, peak (filled) and residual (open) current at the end of 300-ms depolarizations; means of seven cells. Error bars, plotted when larger than symbols, show SEM here and throughout. (**B**) α_{1C} Ca^{2+} currents; the format is identical to that in (A). Records are from the same cell as that in (A) (top); n = 6 cells. (**C**) Residual fraction of peak current, r_{300}, for α_{1C}. The concentration of charge carrier was 10 mM throughout for six cells. The parameter f, subsequently used as a concise descriptor of Ca^{2+} inactivation, is the difference between r_{300} relations at +5 to +10 mV. Isolation of Ca^{2+} channel current, indicated by flat traces near reversal potential [for example, +70 mV in (A), and throughout], is required for quantitative interpretation of r_{300}. Ca^{2+}, solid symbols; Ba^{2+}, open symbols. (**D**) α_{1E} Ba^{2+} currents; the format is identical to that in (A). Top, holding potential, −90 mV; tail potential, −80 mV, with NMG-$MeSO_3$ internal solution (*14*) and 10 mM external Ba^{2+}. Bottom, means of n = 6 cells. (**E**) α_{1E} Ca^{2+} currents; the format is identical to that in (D), with 10 mM external Ca^{2+}. The records are from the same cell as that at the top of (D). The bottom represents results from six cells. (**F**) r_{300} for α_{1E}. The format was identical to that in (C), with 10 mM charge carrier throughout in six cells; symbols are as in (C). The small difference of r_{300} (−30 to 0 mV range) arises from differential screening of surface charge by Ba^{2+} and Ca^{2+}.

Ca^{2+} binding, an EF hand must reside within its own "globular domain" (*22*), which is made of a continuous sequence of amino acids containing the EF hand. The margin between the COOH-termini of α_{1EC-3} and $\alpha_{1EC-1\Delta3}$, amino acids 1650 to 1732 in α_{1C}, may well define a border of such a domain region.

Third, single-channel recordings (*23*) offered a further test of the specificity with which Ca^{2+} inactivation has been removed in the series of α_{1CE} chimeras (collectively denoted as α_{1CE-*}). Work with native L-type Ca^{2+} channels demonstrates that Ca^{2+} inactivation reflects a Ca^{2+}-induced shift in the overall pattern of gating (*10*) from a mode with rapidly activating, high-frequency opening (mode 1), to a mode with slowly activating, infrequent opening (mode Ca). With Ba^{2+}, there is no shift from mode 1 to mode Ca, and mode 1 often predominates. Voltage inactivation renders the channel incapable of opening, yielding depolarizations without activity ("blanks"). Selective knockout of Ca^{2+} inactivation should therefore remove Ca^{2+}-induced shifts to mode Ca but spare the induction of blanks by prolonged depolarization.

Single-channel properties of α_{1C} were compared with those of α_{1CE-1} (Fig. 3), the α_{1CE-*} chimera with the largest change from α_{1C}. Either 10 mM Ba^{2+} or 10 mM Ca^{2+} was used as the charge carrier to enable direct comparison with whole-cell results. The same prepulse protocol (top) was used throughout: depolarizations to +0 mV were alternately preceded by a 0.5-s prepulse to +20 mV or by no prepulse. α_{1C} behaved just as predicted from native L-type Ca^{2+} channels. With Ba^{2+} (Fig. 3A), unitary currents illustrated the predominance of mode 1 gating during test depolarizations with or without prepulse. Ensemble average currents hardly decayed, which is consistent with the absence of Ca^{2+} inactivation. The first latency distribution (F) and conditional open probability (P_{oo}) functions served as quantitative descriptors of these trends (*10*). Values of F plot the probability that a channel first opens by time t after the onset of test depolarization. The rapid rise of F, with and without prepulse, demonstrated the dominance of mode 1 gating throughout. The small depression of the plateau by the prepulse reflected the induction of blank sweeps, which is indicative of voltage inactivation. P_{oo}, the probability of a channel being open at time t after first opening, provided a kinetic fingerprint of gating after first opening. The similarity of values of P_{oo}, with and without prepulse, confirmed the lack of mode shifts. With Ca^{2+} (Fig. 3C), control α_{1C} traces activated rapidly in a bursting pattern, but traces following a prepulse activated slowly in a sparsely opening pattern. Thus, Ca^{2+} entry during the prepulse caused a shift from mode 1 to mode Ca^{2+}, synonymous with Ca^{2+} inactivation. Induction of a slow component in F after the prepulse, as well as depression of P_{oo}, quantitated the shift to mode Ca.

In α_{1CE-1} (Fig. 3, B and D), single-channel properties indicated a selective knockout of Ca^{2+} inactivation. With Ba^{2+} (Fig. 3B), α_{1CE-1} behaved like α_{1C} (compare Fig. 3A); with Ca^{2+} (Fig. 3D), however, there was no shift to mode Ca. The lack of Ca^{2+} inactivation in unitary Ca^{2+} currents excluded differential expression levels as a trivial mechanism for altered inactivation. A final argument against global conformational change came with the similarity of α_{1C} and α_{1CE-1} unitary current amplitudes (≈0.6 and ≈0.25 pA with Ba^{2+} and Ca^{2+}, respectively, for both). This similarity excluded appreciable alteration of permeation.

These results establish the EF-hand motif of α_{1C} as an essential structural determinant of Ca^{2+} inactivation, whereby Ca^{2+} binding to the EF-hand motif initiates Ca^{2+} inactivation. By analogy to other EF hands, the transduction of binding to inactivation might occur by Ca^{2+}-induced exposure of hydrophobic residues on the E and F helices, which could then interact with a complementary hydrophobic surface (*24*) so as to inhibit opening (*10*). "Donation" of the Ca^{2+} inactivation phenotype to $\alpha_{1EC-1\Delta3}$ suggests that the receptor is intact on α_{1E} and that only the binding domain may be defective, as supported by the alignment of the EF-hand regions from the major classes of Ca^{2+} channels (Fig. 4A). For α_{1C} and α_{1D} [which probably has Ca^{2+} inactivation (*25*)], the region is almost identical and these channels score highest (14 out of 16) on a modified Tufty-Kretsinger EF-hand test (*20*). For α_{1E}, α_{1B}, and α_{1A}, which all lack Ca^{2+} inactivation (*26*), divergence is substantial and scores are lower. However, only ≈70% of EF-hand motifs (*27*) actually bind Ca^{2+}; our proposal remains to be confirmed by in vitro methods (*22*).

The location of the EF-hand motif helps explain paradoxical features of the α_{1C} channel. Proximity of the EF hand to the inner lip of the permeation pathway (*28*) predicts insensitivity of Ca^{2+} inactivation to intracellular Ca^{2+} chelators (*29*); diffusion calculations indicate that $[Ca^{2+}]$ in the channel pore would be little affected by such agents (*29*). Conversely, because the EF hand is not

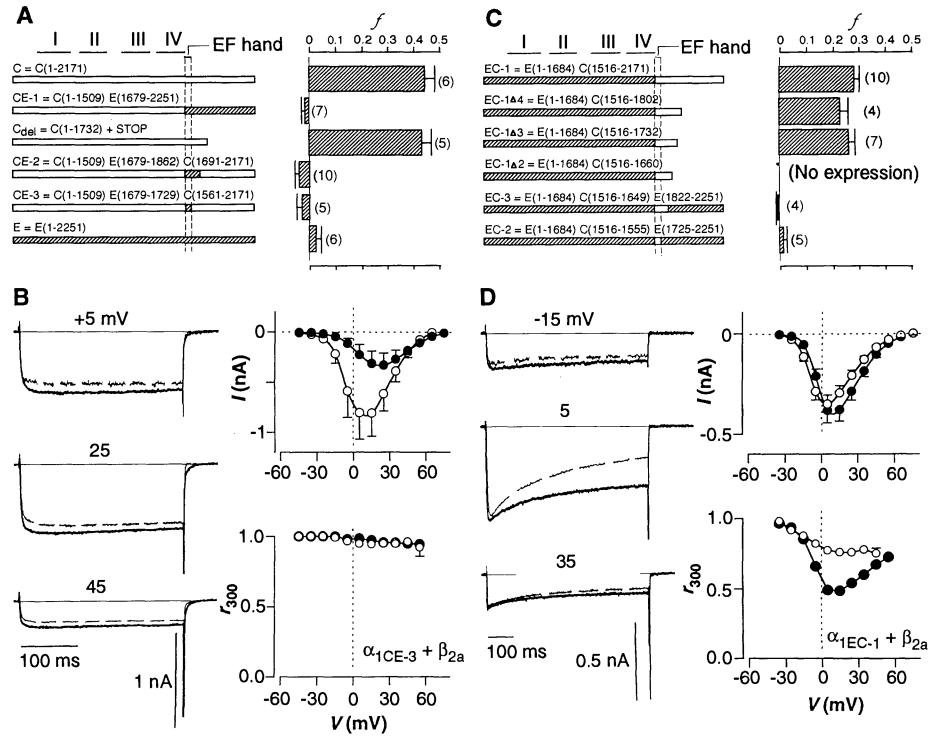

Fig. 2. Molecular determinants of Ca^{2+} inactivation. All α_1 constructs were co-expressed with the β_{2a} subunit to ensure robust expression. (**A**) Left, schematic representation of α_{1C}, α_{1E}, and chimeric constructs (not to scale). Values in parentheses indicate amino acid numbers. Right, corresponding f values (mean ± SEM from the number of cells in parentheses). (**B**) Inactivation of α_{1CE-3}. Left, Ba^{2+} (solid) and Ca^{2+} currents (dashed) during steps to various potentials. Holding potential, −90 mV; tail potential, −80 mV. Ca^{2+} currents were scaled by (from top) 4.38, 2.07, and 0.94 times to facilitate comparison of kinetics. Right, peak current and r_{300} from $n = 5$ cells. Symbols are as in Fig. 1C. (**C**) Schematic representation of α_{1EC-*} chimeric constructs (left) and associated f values (right). The format was identical to that in (A). (**D**) Inactivation of α_{1EC-1}. The format was identical to that in (B). Data are from 10 cells. NMG-$MeSO_3$ internal solution (*14*) was used in (A) through (D); 10 mM charge carrier was used throughout.

quite in the conduction pore, Ca^{2+} inactivation can be accelerated by extra-channel factors, like Ca^{2+} flux through adjacent Ca^{2+} channels (*9*) or ryanodine receptors (*3*). The contiguity of the EF hand to consensus protein kinase A (PKA) phosphorylation sites on the α_{1C} COOH-terminus, regarded as probable loci for channel up-regulation by PKA (*30*), may explain parallels in the mode-shift behavior underlying Ca^{2+} channel regulation by Ca^{2+} and phosphorylation (Fig. 4B). Phosphorylation favors a shift from mode 0_a to mode 1 (*31*), where mode 0_a resembles mode Ca, although L-type Ca^{2+} channels do not require dephosphorylation to inactivate (*10*).

Our findings may have implications for many biological systems, given the wide distribution of L-type Ca^{2+} channels. For example, in heart where the duration of action potentials is highly sensitive to Ca^{2+} inactivation (*32*), the EF-hand region of L-type Ca^{2+} channels is a potential locus for inherited electrical disorders like long QT syndrome (*33*); it also may be a molecular target for new cardiac inotropic and anti-arrhythmic drugs.

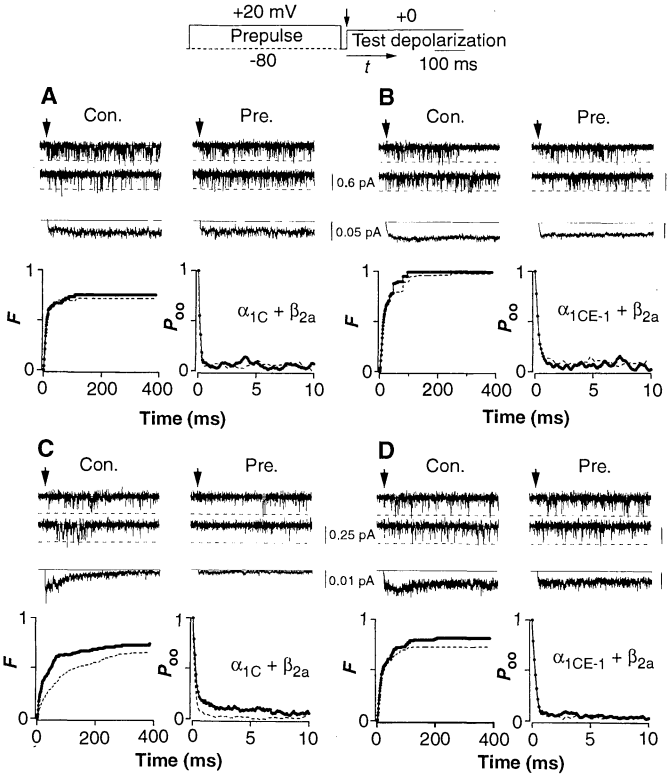

Fig. 3. Single-channel comparison of inactivation in α_{1C} and α_{1CE-1}, both co-transfected with β_{2a}. Top, Voltage-pulse protocol for all panels. Test depolarization lasts 386 ms. (**A**) α_{1C} unitary Ba^{2+} currents. Top, unitary current records from a single patch with two channels filtered at 1400 Hz. Pre., with prepulse; Con., without prepulse control. Dashed lines indicate the open-channel current level. Arrows indicate instant of test depolarization, as indicated by protocol at the top. Middle, ensemble average currents after normalization by the number of channels (here, and in all panels), derived from the same patch. Bottom, first latency distribution (left) and conditional open probability (right), derived from same patch. Solid line, without prepulse; dashed line, with prepulse. (**B**) α_{1CE-1} unitary Ba^{2+} currents. The format is identical to that in (A), with scale bar values as in (A). Shown are exemplar records from a patch with three channels, filtered at 1400 Hz. Ensemble averages, *F*, and P_{oo} were averaged from four patches. (**C**) α_{1C} unitary Ca^{2+} currents. The format is identical to that in (A). Shown are unitary records from a patch with three channels, filtered at 1000 Hz. Ensemble averages, *F*, and P_{oo} were averaged from three patches. (**D**) α_{1CE-1} unitary Ca^{2+} currents. The format was identical to that in (A), with scale bar values as in (C). Shown are records from a patch with two channels, filtered at 700 Hz. Ensemble averages, *F*, and P_{oo} are averaged from four patches.

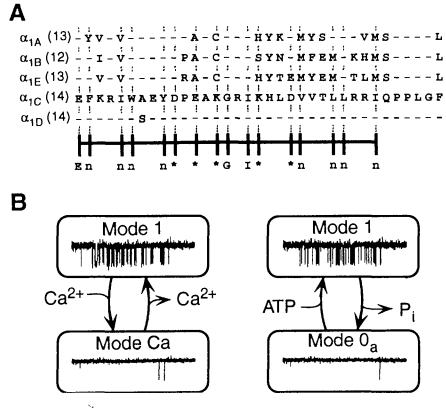

Fig. 4. Mechanistic features of Ca^{2+}-sensitive inactivation. (**A**) Alignment of EF-hand regions from five major classes of voltage-gated Ca^{2+} channels (*35*). Shown are amino acids 1782 to 1816 of α_{1A} (*36*), 1728 to 1762 of α_{1B} (*37*), 1695 to 1729 of α_{1E} (*16*), 1526 to 1560 of α_{1C} (*12*), and 1495 to 1529 of α_{1D} (*38*). Dashes show positions of identity to α_{1C} (*39*). For reference, the modified Tufty-Kretsinger scoring template (*20*) is shown at the bottom, with scoring numbers in parentheses above. Residues E, G, and I are the anticipated amino acids in this position of an EF hand. "n" denotes a hydrophobic amino acid (L, I, V, F, M, W, and Y), and the asterisk denotes a ligand vertex for Ca^{2+} (D, N, E, Q, S, and T). Each such criterion that is satisfied contributes one point; the score of each channel appears in parentheses. (**B**) Parallels in the gating modes underlying Ca^{2+} channel regulation by Ca^{2+} and PKA phosphorylation. Simulated traces are for illustration only. P_i, inorganic phosphate.

REFERENCES AND NOTES

1. P. Brehm and R. Eckert, *Science* **202**, 1203 (1978).
2. H. Scherubl *et al.*, *Am. J. Physiol.* **264**, E354 (1993).
3. J. Sham and M. Morad, *Proc. Natl. Acad. Sci. U.S.A.* **92**, 121 (1995).
4. M. Sheng, G. McFadden, M. E. Greenberg, *Neuron* **4**, 571 (1990).
5. J. E. Chad and R. Eckert, *J. Physiol. (London)* **378**, 31 (1986).
6. D. L. Armstrong, *Trends Neurosci.* **12**, 117 (1989).
7. A. Sherman, J. Keizer, J. Rinzel, *Biophys. J.* **58**, 985 (1990).
8. D. T. Yue, P. H. Backx, J. P. Imredy, *Science* **250**, 1735 (1990); J. A. Haack and R. L. Rosenberg, *Biophys. J.* **66**, 1051 (1994).
9. J. P. Imredy and D. T. Yue, *Neuron* **9**, 197 (1992).
10. ———, *ibid.* **12**, 1301 (1994).
11. R. H. Kretsinger, *Nature* **240**, 85 (1972).
12. X. Wei *et al.*, *J. Biol. Chem.* **266**, 21943 (1991); X. Wei *et al.*, *ibid.* **269**, 1635 (1994).
13. E. Perez-Reyes *et al.*, *ibid.* **267**, 1792 (1992).
14. Complementary DNAs encoding α_{1C} (*12*), α_{1E} (*34*), and β_{2a} (*13*) were subcloned into pGW1H (British Biotechnologies, Oxford), an expression plasmid with a cytomegalovirus promotor. HEK 293 cells were transiently transfected as described (*34*), with the use of α_1 and β_{2a} constructs (10 mg each per 100-mm plate). Whole-cell currents were recorded at room temperature by patch-clamp techniques with the use of an Axopatch 200A (Axon Instruments, Foster City, CA). The bath solution contained 130 mM *N*-methyl-d-glucamine (NMG) aspartate, 1 mM $MgCl_2$, 10 mM glucose, 10 mM 4-aminopyridine, 10 mM Hepes, and 10 mM $BaCl_2$ or $CaCl_2$ (pH 7.3), adjusted with NMG. The internal solution was based on either Cs-aspartate or NMG-methanesulfonate ($MeSO_3$). The Cs-aspartate solution contained 135 mM Cs-aspartate, 5 mM CsCl, 5 mM EGTA, 1 mM $MgCl_2$, 4 mM Mg adenosine triphosphate (ATP), and 10 mM Hepes (pH 7.3), adjusted with CsOH. NMG-$MeSO_3$ solution contained 140 mM NMG-$MeSO_3$, 5 mM EGTA, 1 mM $MgCl_2$, 4 mM MgATP, and 10 mM Hepes (pH 7.3), adjusted with NMG. Results with NMG-$MeSO_3$ internal solution were adjusted by +15 mV to account for the junction potential difference with Cs-aspartate internal solution. Series resistance was typically <10 megohms and was compensated by 70%. Leak and capacitance currents were subtracted by a P/8 protocol [C. M. Armstrong and F. Bezanilla, *J. Gen. Physiol.* **63**, 533 (1974)]. Voltage pulses were delivered every 15 to 20 s, and data were sampled at 10 kHz and filtered at 2 kHz (−3 dB, 4-pole Bessel). Smooth curves were fitted by eye here and throughout.
15. H. Reuter, *Prog. Biophys. Mol. Biol.* **26**, 1 (1973).
16. T. W. Soong *et al.*, *Science* **260**, 1133 (1993).
17. α_{1C} expressed alone yielded Ca^{2+} currents with Ca^{2+} inactivation properties similar to those of $\alpha_{1C} + \beta_{2a}$ (Fig. 1C), although expression levels were considerably smaller.
18. A. Welling *et al.*, *Circ. Res.* **73**, 974 (1993).
19. r_{300} relations were no different with 3 mM and 10 mM Ba^{2+} or Ca^{2+} as the charge carrier.
20. J. Babitch, *Nature* **346**, 321 (1990).
21. Chimeric Ca^{2+} channels were constructed by ligating polymerase chain reaction (PCR) products, derived from a "donor" channel, into selected restriction endonuclease sites on a "recipient" channel. PCR primers contained corresponding restriction endonuclease sites. All chimeras were subcloned into pGW1H. Methods are as follows. The chimera α_{1CE-1} contains nucleotides 1 to 4492 from α_{1C} (α_{1C}:

1 to 4492) and nucleotides 5000 to 6756 from α_{1E} (α_{1E}: 5000 to 6756), with position 1 at the start codon; the α_{1E} fragment was ligated into α_{1C} that had been cut at nucleotide position 4487 with Bcl I, and in the polylinker with Xba I. For α_{1Cdel} (α_{1C}: base pairs 1 to 5196 + TAG), the Bst EII (α_{1C}: 4641) and Xba I (polylinker) region of α_{1C} was replaced with a shorter fragment, including a premature stop codon after the codon for amino acid 1732. For α_{1CE-2} (α_{1C}: 1 to 4492 and α_{1E}: 5000 to 5586 and α_{1C}: 5071 to 6516), the α_{1C} fragment (α_{1C}: 5071 to 6516) was ligated into Sau I (α_{1CE-1}: 5071) and Xba I (polylinker) of α_{1CE-1}. For α_{1CE-3} (α_{1C}: 1 to 4492 and α_{1E}: 5000 to 5187 and α_{1C}: 4681 to 6516), the α_{1C} fragment (α_{1C}: 4681 to 6516) was ligated into Stu I (α_{1CE-1}: 4674) and Xba I (polylinker) of α_{1CE-1}. For α_{1EC-1} (α_{1E}: 1 to 5050 and α_{1C}: 4544 to 6516), the α_{1C} fragment (α_{1C}: 4544 to 6516) was ligated into the Xho I (α_{1E}: 5045) and Sal I (polylinker) sites of α_{1E}. For $\alpha_{1EC-1\Delta4}$ (α_{1E}: 1 to 5050 and α_{1C}: 4544 to 5406 + TAG), the α_{1EC-1} fragment (α_{1EC-1}: 4299 to 5913 + TAG) was ligated into the Bst 1107I (α_{1EC-1}: 4299) and Sal I (polylinker) sites of α_{1EC-1}. For $\alpha_{1EC-1\Delta3}$ (α_{1E}: 1 to 5050 and α_{1C}: 4544 to 5196 + TAG), the α_{1EC-1} fragment (α_{1EC-1}: 4299 to 5703 + TAG) was ligated into the Bst 1107I (α_{1EC-1}: 4299) and Sal I (polylinker) sites of α_{1EC-1}. For $\alpha_{1EC-1\Delta2}$ (α_{1E}: 1 to 5050 and α_{1C}: 4544 to 4980 + TAG), the α_{1EC-1} fragment (α_{1EC-1}: 4299 to 5487 + TAG) was ligated into the Bst 1107I (α_{1EC-1}: 4299) and Sal I (polylinker) sites of α_{1EC-1}. For α_{1EC-3} (α_{1E}: 1 to 5050 and α_{1C}: 4544 to 4947 and α_{1E}: 5464 to 6756), the α_{1E} fragment (α_{1E}: 5464 to 6756) was ligated into Bgl II (α_{1EC-1}: 5369) to Sal I (polylinker) of α_{1EC-1}. For α_{1EC-2} (α_{1E}: 1 to 5050 and α_{1C}: 4544 to 4667 and α_{1E}: 5175 to 6756), the α_{1E} fragment (α_{1E}: 5175 to 6756) was ligated into Bst EII (α_{1EC-1}: 5148) and Sal I (polylinker) of α_{1EC-1}. Portions of chimeric channel constructs derived from PCR were verified in their entirety with the use of the fluorescent dideoxy terminator method of thermocycle sequencing on an automated DNA sequencer (Perkin-Elmer, Applied Biosystems Division 373a).

22. P. Brodin, C. Johanson, S. Forsén, T. Drakenberg, T. Grundstrom, *J. Biol. Chem.* **265**, 11125 (1990); S. Linse, A. Helmersson, S. Forsén, *ibid.* **266**, 8050 (1991); S. Linse and S. Forsén, *Adv. Second Messenger Phosphoprotein Res.* **30**, 89 (1995).
23. Single-channel currents were recorded at room temperature by on-cell patch-clamp (*10*). Bath solution consisted of 132 mM potassium glutamate, 5 mM KCl, 5 mM NaCl, 3 mM $MgCl_2$, 2 mM EGTA, 1 mM CaATP, 10 mM glucose, and 10 mM Hepes (pH 7.3), adjusted with KOH. Pipette solution consisted of 10 mM $BaCl_2$ or 10 mM $CaCl_2$, 100 mM tetraethylammonium (TEA) chloride, and 10 mM Hepes (pH 7.4), adjusted with TEA-OH. Voltage pulses were delivered every 5 to 8 s. The integrating headstage of Axopatch 200A was used. Data were sampled at 10 kHz and filtered at 1 to 2 kHz (for Ba^{2+} data) and at 0.7 to 1 kHz (for Ca^{2+} data) (−3 dB, 4-pole Bessel). The average current, F, and P_{oo} were analyzed as described (*10*).
24. N. C. J. Strynadka and M. N. G. James, *Annu. Rev. Biochem.* **58**, 951 (1989).
25. S. Seino *et al.*, *Proc. Natl. Acad. Sci. U.S.A.* **89**, 584 (1992); T. D. Plant, *J. Physiol. (London)* **404**, 731 (1988).
26. $\alpha_{1B} + \beta_{2a}$ showed identical r_{300} curves with 10 mM Ba^{2+} or 10 mM Ca^{2+} as the charge carrier; W. A. Sather *et al.*, *Neuron* **11**, 291 (1993).
27. H. Kawasaki and R. Kretsinger, *Protein Profile* **1**, 343 (1994).
28. D. S. Ragsdale, J. C. McPhee, T. Scheuer, W. A. Catterall, *Science* **265**, 1724 (1994).
29. M. J. Gutnick, H. D. Lux, D. Swandulla, H. Zucker, *J. Physiol. (London)* **412**, 197 (1989).
30. A. Yoshida, M. Takahashi, S. Nishimura, H. Takeshima, S. Kokubun, *FEBS Lett.* **309**, 343 (1992).
31. D. T. Yue, S. W. Herzig, E. Marban, *Proc. Natl. Acad. Sci. U.S.A.* **87**, 753 (1990).
32. D. Noble, *The Initiation of the Heartbeat* (Clarendon, Oxford, 1979), pp. 1–186.
33. Q. Wang *et al.*, *Cell* **80**, 1 (1995).
34. R. S. Dhallan, K.-W. Yau, K. A. Schrader, R. R. Reed, *Nature* **347**, 184 (1990).
35. Abbreviations for the amino acid residues are as follows: A, Ala; C, Cys; D, Asp; E, Glu; F, Phe; G, Gly; H, His; I, Ile; K, Lys; L, Leu; M, Met; N, Asn; P, Pro; Q, Gln; R, Arg; S, Ser; T, Thr; V, Val; W, Trp; and Y, Tyr.
36. T. V. B. Starr, P. Ward, T. P. Snutch, *Proc. Natl. Acad. Sci. U.S.A.* **88**, 5621 (1991).
37. S. J. Dubel *et al.*, *ibid.* **89**, 5058 (1992).
38. M. E. Williams *et al.*, *Science* **257**, 389 (1992).
39. α_{1CE-3} differs from α_{1C} by two other amino acids not included in the alignment in Fig. 4A. Both are located just NH_2-terminal to the EF hand: E for D in α_{1C} (*35*), and S for W in α_{1C}, at positions 1510 and 1516, respectively, of α_{1CE-3}. Neither of these differences would be expected to alter Ca^{2+} binding to the EF hand. In fact, α_{1EC-1}, $\alpha_{1EC-1\Delta3}$, and $\alpha_{1EC-1\Delta4}$ reconstitute Ca^{2+} inactivation but maintain the E at position 1510.
40. We thank J. P. Imredy, P. G. Patil, D. L. Brody, B. A. Lewis, and K. W. Yau for discussion and comments; S. Sisodia and M. Schlissel for molecular biological advice; and the DNA Analysis Facility of Johns Hopkins for sequencing. Supported by grants from NIH (D.T.Y. and E.P.-R.) and the Medical Research Council of Canada and the Howard Hughes Medical Institute (T.P.S.); an Established Investigatorship of the American Heart Association (D.T.Y.); a Medical Scientist Training Program award (L.J.); and a National University of Sing- apore fellowship (T.W.S.).

23 March 1995; accepted 13 October 1995

Coactivator and Promoter-Selective Properties of RNA Polymerase I TAFs

Holger Beckmann, Jin-Long Chen, Thomas O'Brien, Robert Tjian*

Human ribosomal RNA synthesis by RNA polymerase I requires the activator UBF and the promoter selectivity factor SL1, which consists of the TATA binding protein (TBP) and three associated subunits, TAF_I110, TAF_I63, and TAF_I48. Here it is shown that both TAF_I110 and TAF_I63 contact the promoter, whereas TAF_I48 serves as a target for interaction with UBF and is required to form a transcriptionally active SL1 complex responsive to UBF in vitro. TAF_I48 also alters the ability of TBP to interact with TATA box elements, and the resulting complex fails to support transcription by RNA polymerase II. Thus, TAF_I48 may function both as a target to mediate UBF activation and as a class-specific promoter selectivity factor.

Enhancement of transcription initiation by sequence-specific DNA binding proteins is a principal mechanism for regulating gene expression in animal cells (*1*). Promoter-selective transcriptional activators bind DNA and interact with specific components of the basal transcriptional apparatus in order to modulate gene expression (*2*). For example, some site-specific enhancer binding proteins directly target subunits of the basal transcription factor TFIID, which consists of TBP and at least eight TBP-associated factors called TAF_{II}s (*3–8*). Transcription of the human 18S and 28S ribosomal RNA genes by RNA polymerase I (RNA Pol I) also requires a TBP-TAF complex called selectivity factor 1 (SL1). All four subunits (TBP, TAF_I48, -63, and -110) are necessary to form an SL1 complex that supports transcription in vitro with purified RNA Pol I and the upstream binding factor, UBF (*9–11*). Consequently, one or more TAFs in the SL1 complex are expected to recognize and bind core promoter DNA, whereas other subunits may be targets for activation by UBF.

To test the activator binding properties of individual TAFs in the SL1 complex, we performed protein-protein binding assays with an affinity resin containing human recombinant UBF (rUBF) (Fig. 1) (*12*). As reported previously, UBF interacts with TBP (*13*). However, TBP alone is unable to support UBF-dependent activation of transcription by RNA Pol I (*11*). We therefore tested each of the TAFs associated with

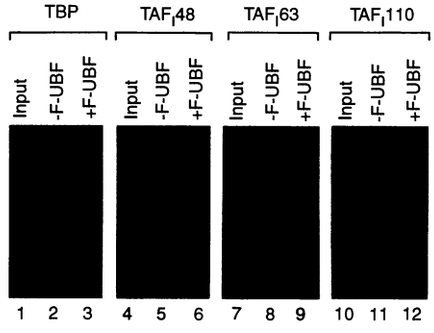

Fig. 1. TAF_I48 subunit of the SL1 complex binds to UBF. Partially purified FLAG epitope–tagged UBF (*12*) was immobilized on protein A–Sepharose beads conjugated with antibodies directed against the FLAG epitope (*10*). This resin (lanes 3, 6, 9, and 12) and resins containing the antibodies but lacking UBF (lanes 2, 5, 8, and 11) were incubated with in vitro ^{35}S-methionine–labeled TBP (lanes 2 and 3), TAF_I48 (lanes 5 and 6), TAF_I63 (lanes 8 and 9), and TAF_I110 (lanes 11 and 12). Bound proteins were resolved by SDS-PAGE and visualized by autoradiography (*10*). Lanes 1, 4, 7, and 10 show 10% of the individual TAFs used in the binding assay.

Howard Hughes Medical Institute, Department of Molecular and Cell Biology, University of California, Berkeley, CA 94720–3204, USA.

*To whom correspondence should be addressed.